

# Magnetic response of mesoscopic superconducting rings with two order parameters

Hendrik Bluhm,<sup>1,\*</sup> Nicholas C. Koshnick,<sup>1</sup> Martin E. Huber,<sup>2</sup> and Kathryn A. Moler<sup>1</sup>

<sup>1</sup>*Departments of Physics and Applied Physics, Stanford University, Stanford, CA 94305*

<sup>2</sup>*Department of Physics, University of Colorado at Denver, Denver, CO 80217*

(Dated: 08/10/06)

The magnetic response and fluxoid transitions of superconducting aluminum rings of various sizes, deposited under conditions likely to generate a layered structure, show good agreement with a two-order-parameter Ginzburg-Landau model. The experimentally determined coupling strength between the two order parameters depends on the line width. For intermediate couplings, we find metastable states that have different phase winding numbers around the ring in each of the two order parameters.

PACS numbers: 74.78.Na, 74.45.+c, 74.78.Fk, 74.20.De

Since the discovery of two-gap superconductivity in MgB<sub>2</sub> [1], the coexistence of two not-too-strongly coupled superconducting order parameters (OPs) has motivated significant theoretical work. A striking prediction is the existence of vortices carrying unquantized flux [2]. In a ring geometry, those correspond to a soliton-like spatial variation of the phase difference between the two OPs [3]. We have observed those states and other phenomena arising from the interplay between two OPs in rings consisting of two parallel Josephson-coupled thin film layers. Our results can be described by two-OP Ginzburg-Landau (GL) theory [4], a model that applies for both a tunneling BCS Hamiltonian and intrinsic two-gap superconductivity [5].

We used a scanning SQUID microscope (SSM) [6] to study mesoscopic superconducting aluminum rings fabricated on a single chip. Positioning the SQUID over each ring individually enabled measurements of the current,  $I$ , circulating the ring as a function of applied flux,  $\Phi_a$ , and temperature,  $T$ . The ensemble of magnetic responses includes distinct features that cannot be explained by one-OP GL, but can be described by numerical solutions of two-OP GL. The inferred coupling between the two OPs depends on the ring's annulus width,  $w$ , allowing us to study the crossover between intermediate and strong coupling regimes. For intermediate coupling, metastable states with different phase winding numbers for each OP exist, corresponding to the solitons predicted in Ref. [3]. In this regime, there are multiple transition pathways between states, giving a rich structure of hysteretic  $\Phi_a - I$  curves. At stronger coupling, the system approaches the Cooper limit of complete proximitization [7]: the  $\Phi_a - I$  curves at any temperature can be described by one-OP GL, but the existence of two OPs is manifest in the temperature dependence of the fitted penetration depth,  $\lambda$ , and the GL-coherence length,  $\xi_{GL}$ .

During the course of a single two-month-long cooldown, we characterized the magnetic response of 40 different rings with eight annulus widths  $45 \text{ nm} \leq w \leq 370 \text{ nm}$  and radii  $R$  of 0.5, 0.8, 1.2 and 2  $\mu\text{m}$ . The rings were fabricated on oxidized silicon, using liftoff lithogra-

phy with PMMA resist. The 40 nm thick aluminum film was deposited by e-beam evaporation at a rate of about 1  $\text{\AA/s}$  and a pressure of approximately  $10^{-6}$  mBar. During the deposition, the rate temporarily dropped to a negligible level for about 10 min and subsequently recovered, which most likely caused the formation of two superconducting layers separated by an AlO<sub>x</sub> tunneling barrier. A disk with a radius of 2  $\mu\text{m}$  had a  $T_c$  of 1.6 K, representative of the bulk film. Using  $\xi_0 = 1.6 \mu\text{m}$  for pure bulk Al [8] and  $\xi_{GL}(0) \approx 70 \text{ nm}$  for our rings, as derived below, we infer a mean free path of  $l_e = 1.4\xi_{GL}(0)^2/\xi_0 = 4 \text{ nm}$ . The measured critical temperatures  $T_c$  of the rings ranged from 1.5 to 1.9 K, depending only on  $w$ . Both the short  $l_e$  and the large  $T_c$  compared to clean bulk Al indicate small grains and a (likely related) strong effect of oxygen impurities [9, 10].

Our SSM operates in a magnetically shielded dilution refrigerator [6], modified to be stable up to 2 K, with a piezo scanner [11] and a commercial coarse motion stage [12]. The SQUID sensor [13], which is aligned to be nearly parallel to the sample, has a 4  $\mu\text{m}$  diameter pickup loop and a flux sensitivity better than  $1 \mu\Phi_0/\sqrt{\text{Hz}}$ , with a pickup loop - ring inductance  $M_{coup} = 0.1 - 1 \Phi_0/\text{mA}$ , depending on  $R$ . A concentric 13  $\mu\text{m}$  diameter field coil applies a local field. A symmetric second pair of loops allows nulling of the SQUID response to the applied field to  $\sim 1 \text{ m}\Phi_0$ . We position the pickup loop over a ring, record time traces of the SQUID response while sinusoidally varying  $\Phi_a$  at a few Hz, and average hundreds to thousands of field sweeps. Roughly once a minute, the SQUID is retracted to measure a background, which is subtracted. The remaining signal is the flux generated by  $I$  plus a residual sensor background of about 0.1 m $\Phi_0$ , consisting of a constant and in- and out-of-phase components at the frequency of  $\Phi_a$ . This residual background is negligible at lower  $T$  and unambiguously distinguishable from the ring response at higher  $T$ , where fluxoid transitions occur. The non-scanning approach of comparable previous high sensitivity susceptibility measurements [14, 15, 16] would not allow measurement of either the background or many samples per cooldown.

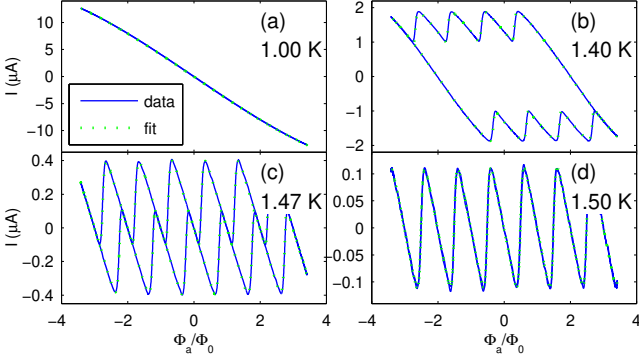


FIG. 1:  $\Phi_a - I$  curves for a ring with  $w = 120$  nm and  $R = 1.2 \mu\text{m}$ , fitted to a one-order-parameter Ginzburg-Landau model. The selected curves represent the regimes discussed in the text: (a) no transitions, (b), (c) hysteretic and (d) thermal equilibrium.

Rings with  $w \leq 120$  nm show no two-OP effects [Fig. 1]. At low  $T$  [Fig. 1(a)], there are no fluxoid transitions at the experimental time scale and field sweep amplitude. At higher  $T$  [Fig. 1(b), (c)], we observe hysteretic transitions, which become non-hysteretic near  $T_c$  [Fig. 1(d)].

We obtain the theoretical  $\Phi_a - I$  curve of an individual fluxoid state,  $n$ , directly from 1D, 1-OP GL [16]:

$$I_n(\varphi) = -\frac{wd\Phi_0}{2\pi R\mu_0\lambda^2}(\varphi - n) \left(1 - \frac{\xi_{GL}^2}{R^2}(\varphi - n)^2\right) \quad (1)$$

where  $\varphi = \Phi_a/\Phi_0$ ,  $\Phi_0 = h/2e$ , and  $n$  is the phase winding number of the GL-OP  $\psi(x) = |\psi|e^{inx/R}$ , where  $x$  is the distance around the ring's circumference.  $\varphi \ll \xi_{GL}/R$  gives the linear response of the London limit, while the cubic term arises from pair breaking. Because  $wd \ll \lambda^2$ , the self inductance can be neglected. Although the width of some rings is several  $\xi_{GL}$  at low  $T$ , the 1D approximation is justified here because  $H_a \ll H_{c2}$  [16].

Close to  $T_c$  [Fig. 1(d)], transitions are fast enough to model the experimental  $\Phi_a - I$  curves as a thermal average over all possible states,

$$\langle I(\varphi) \rangle = \frac{\sum_n I_n(\varphi) e^{-E_n(\varphi)/k_B T}}{\sum_n e^{-E_n(\varphi)/k_B T}} \quad (2)$$

with  $E_n(\varphi) = \Phi_0 \int_0^\varphi d\varphi' I_n(\varphi')$ . We set  $\xi_{GL} = 0$  when substituting Eqn. (1) into Eqn. (2) because the thermal rounding dominates the cubic term [23]. The seven free parameters in the fit are  $\lambda^{-2}$ , three background parameters, and three calibration factors: a small offset in  $\varphi$ , the pickup loop - ring inductance  $M_{coup}$ , and the field coil - ring inductance. The fitted calibration factors are consistent with less accurate geometrical estimates, and are used at lower  $T$ . From comparing nominally identical rings and the reproducibility of the temperature dependence, we estimate a systematic error of up to 20 % in

$M_{coup}$ , which is mainly due to drift of the piezo scanner and results in a 20 % error in  $\lambda^{-2}$ .

Transitions in the hysteretic curves [Fig. 1(b), (c)] due to thermally activated phase slips [17] are rounded from averaging over a distribution of transitions near a typical  $\phi = \phi_t + n$ . We model such curves by combining Eqn. (1) with occupation probabilities  $p_n(\varphi - n)$  obtained from integrating the rate equation  $dp_n/dt = -p_n/\tau_0 \exp(-E_{act}(\varphi - n)/k_B T)$ . For fitting,  $\tau_0$  and the activation energy  $E_{act}$  are absorbed into  $\phi_t$ . The model is fitted with seven free parameters corresponding to  $\phi_t$ ,  $dE_{act}/d\varphi(\phi_t)$ ,  $\xi_{GL}$ ,  $\lambda^{-2}$ , and three background parameters.

For  $T \ll T_c$ , where no transitions are seen, Eqn. (1) fits the data with three parameters corresponding to  $\xi_{GL}$ ,  $\lambda^{-2}$ , and a constant background.

The above models result in excellent fits for measured  $\Phi_a - I$  curves except at  $w = 190$  nm as discussed below. The fitted values for  $\lambda^{-2}$  and  $\xi_{GL}$  are shown in Fig. 2 for rings typical of each  $w$ . All 14 measured rings with  $w \leq 120$  nm show  $T$ -dependence similar to the 1-OP phenomenological expressions  $\lambda(T)^{-2} = \lambda(0)^{-2}(1 - t^4)$  and  $\xi_{GL}(T) = \xi_{GL}(0)\sqrt{(1 + t^2)/(1 - t^2)}$ , with  $t = T/T_c$ . For  $w \geq 190$  nm,  $\lambda^{-2}(T)$  has a high-temperature tail to an enhanced  $T_c$  and a peak in  $\xi_{GL}$  near but below  $T_c$ . Both effects are most pronounced at  $w = 190$  nm. The  $\Phi_a - I$  curves remain hysteretic well into the tails, showing that the enhanced  $T_c$  is not a fluctuation effect.

The most striking features of the  $\Phi_a - I$  curves for a  $w = 190$  nm ring [Fig. 3(a)-(f)], typical for all six measured rings with  $w = 190$  nm and  $R \geq 1.7 \mu\text{m}$ , are reentrant hysteresis and transition points in the lower  $T$  hysteretic region that are not a function of  $\varphi - n$  only [24]. The former is qualitatively related to the local maximum in  $\xi_{GL}(T)$  [Fig. 2(b)], since in 1-OP GL, a state becomes unstable at  $|\varphi - n| \geq \sqrt{R^2 + \xi_{GL}^2/2}/\sqrt{3}\xi_{GL}$  [18]. However, rather than the transitions shifting to larger values of  $\varphi$  upon raising  $T$ , as one would expect for a decreasing  $\xi_{GL}(T)$ , the amplitude of those transitions is reduced until a non-hysteretic curve with a flattening too pronounced to be described by Eqn. (1) [Fig. 3(d)] appears. With a further increase of  $T$  [Fig. 3(e), (f)] this flattening also disappears and the  $\Phi_a - I$  curves evolve similarly to Fig. 1. This strongly suggests the existence of two OPs, one causing the small ripples in Fig. 3(c), and one with a larger  $T_c$  adding the large background response and causing the tail in  $\lambda^{-2}(T)$ . The additional phase winding number from a second, coupled OP also explains the irregular transitions in [Fig. 3(a)-(c)]. Although also breaking strict flux periodicity, the effect of finite line width corrections to 1D, 1-OP GL [16] would be much smaller and more regular.

A two-OP GL-model consisting of two standard 1D GL free energy functionals and a coupling term indeed

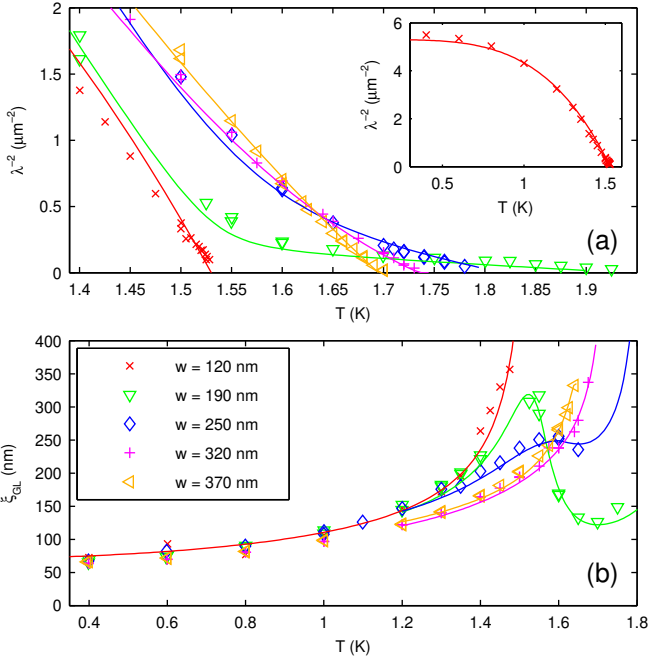


FIG. 2: (a)  $\lambda^{-2}$  and (b)  $\xi_{GL}$  for rings representative of each annulus width  $w$ . The discrete symbols are obtained from fits to  $\Phi_a - I$  curves. Continuous curves represent fits to phenomenological expressions ( $w = 120$  nm) or the two-order-parameter GL model ( $w \geq 190$  nm), which was only fitted above 1.2 K where GL applies.

reproduces the peculiar features of Fig. 2 and 3:

$$F[\psi_1, \psi_2, \varphi] = F_1[\psi_1, \varphi] + F_2[\psi_2, \varphi] + \frac{\gamma w}{2} \int_0^L dx |\psi_1 - \psi_2|^2 \quad \text{with} \quad (3)$$

$$F_i[\psi_i, \varphi] = w d_i \int_0^L dx \left\{ \frac{\hbar^2}{2m} \left| \left( -i \nabla + \frac{\varphi}{R} \right) \psi_i \right|^2 + \frac{\alpha_i}{2} |\psi_i|^2 + \frac{\beta_i}{4} |\psi_i|^4 \right\} \quad (4)$$

We define  $\psi_1$  to have the lower  $T_c$ . If both components have the same  $n$ , one can make the usual ansatz  $\psi_i(x) = |\psi_i| e^{inx/R}$ . Minimizing (3) with respect to  $|\psi_1|$  and  $|\psi_2|$  results in excellent fits to  $\Phi_a - I$  curves as in Fig. 3(d). At small  $\varphi$ , both OPs contribute significantly, but as  $\varphi$  is increased, pair breaking strongly reduces  $|\psi_1|$ , whose  $\xi_{GL}$  diverges near  $T_{c,1}$ . In the absence of the more stable  $\psi_2$ ,  $\psi_1$  would undergo a fluxoid transition much before  $|\psi_1|$  could be suppressed that much.

We extracted effective values of  $\lambda^{-2}(T)$  and  $\xi_{GL}(T)$  from such modeled  $\Phi_a - I$  curves (and also from fits to datasets similar to Fig. 3(d)) using a small  $\varphi$  expansion analogous to Eqn. (1). Assuming a linear  $T$ -dependence of  $\alpha_1$  and  $\alpha_2$ , this procedure can reproduce the observed form of  $\lambda^{-2}(T)$  and  $\xi_{GL}(T)$  as demonstrated by the fits in Fig. 2. The knee in  $\lambda^{-2}(T)$  corresponds to the lower  $T_{c,1}$ ,

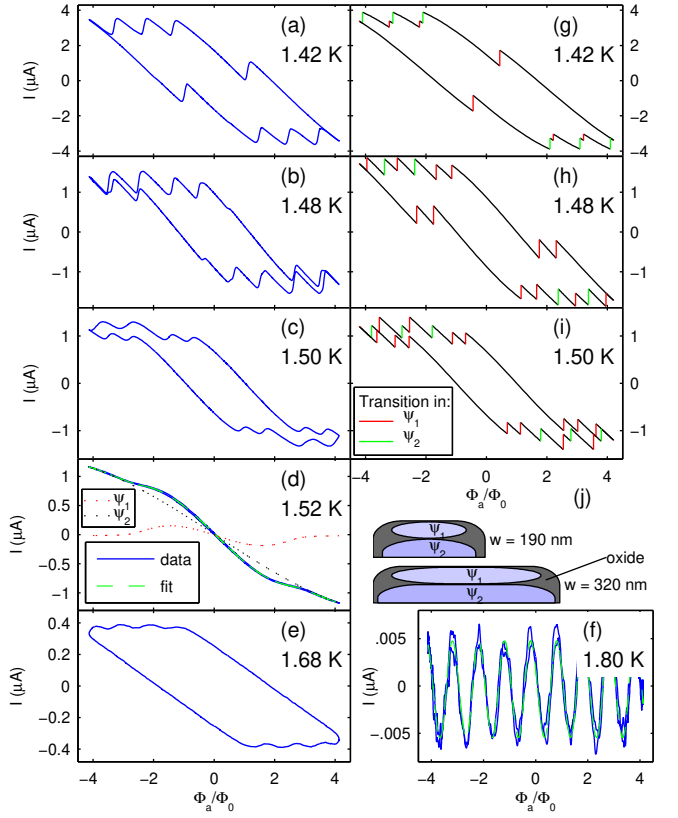


FIG. 3: (a)-(f):  $\Phi_a - I$  curves for a ring with  $w = 190$  nm and  $R = 2 \mu\text{m}$  where the coupling between the two order parameters is weak. In (a) - (c), states with two different fluxoid numbers lead to the observed transition pattern. In (d), no transition occurs because one component is stabilized by the other. Dotted lines show the contributions of  $\psi_1$  and  $\psi_2$  derived from the model. (g)-(i): Results from the two-OP model corresponding to (a)-(c). (j): Schematic of film structure (cross section).

above which the amplitude of  $\psi_1$  becomes very small. From  $w = 190$  nm to  $w = 370$  nm, the coupling strength  $\gamma$  increases by a factor 30-50, by far the largest line width dependence of all fit parameters[25]. The increased coupling causes a stronger proximitization, which smears out the two-OP features with increasing  $w$ . It appears that  $\psi_1$  not only has a lower  $T_c$ , but also a smaller  $l_e$  than  $\psi_2$ . Fit parameters obtained from  $\Phi_a - I$  curves and the curves in Fig. 2 are consistent within about a factor 2. It is conceivable that this discrepancy is caused by fluctuations of  $\psi_1$  at large  $\varphi$ , which have not been included in our model for  $\Phi_a - I$  curves.

To model the hysteretic  $\Phi_a - I$  curves [Fig. 3(a)-(c)], we calculate the activation energies  $E_{act}(\varphi - n)$  for transitions in either  $\psi_1$  or  $\psi_2$  by numerically computing saddle point solutions of the GL - equations obtained from variation of (3), assuming that the relevant saddle points evolve continuously from those of the uncoupled system upon increasing  $\gamma$ . We then derive the complete  $\Phi_a - I$

curve assuming that a transition in  $\psi_i$  occurs whenever  $E_{act}(\varphi - n) < \kappa_i k_B T$ , where the  $\kappa_{1,2}$  are treated as phenomenological parameters of order unity. Of several simulation runs with various parameters similar to those obtained from the fits, the one shown in Fig. 3(g)-(i) gave the best similarity with the data [Fig. 3(a)-(c)]. While the uncertainty of the fit parameters [25] and simplicity of the model forbid a more quantitative comparison, the simulations show that metastable states with  $n_1 \neq n_2$  are key to understanding the observed  $\Phi_a - I$  curves. Due to the coupling between the OPs, the variation of the relative phase is soliton-like [3], similar to a Josephson vortex, however with the phase gradient along the junction being mostly due to the kinetic rather than the magnetic inductance. This soliton corresponds to the domain walls originating from unquantized vortices in bulk samples [2]. Intuitively, it is formed upon increasing  $\varphi$  when the larger  $\xi_{GL}$  of  $\psi_1$  causes  $\psi_1$  to become unstable at a smaller  $\varphi$  than  $\psi_2$ , and the coupling is weak enough for  $\psi_2$  to stay in the same state when this transition occurs. However, due to the energy cost of the phase difference, it is less stable than states with  $n_1 = n_2$ . This leads to the observed step-like structure of the transition sequence.

Apart from the general agreement with the simulations and the irregular transitions, the most direct experimental evidence for the soliton states are branches of  $\Phi_a - I$  curves that are shifted relative to each other by less than one  $\Phi_0$  horizontally, such as around  $\Phi_a/\Phi_0 \approx \pm 3$  in Fig. 3(b). Individual, unaveraged field sweeps show that this is not an effect of averaging over different transition pathways, contrary to the features at  $\Phi_a/\Phi_0 \approx \pm 0.3$ .

We believe that the emergence of two OPs can be explained by the temporary drop of the deposition rate during the metalization. At the lower rate, more oxygen would have been co-deposited to form a tunneling barrier [see Fig. 3(j)]. Different oxygen concentrations and/or grain sizes could have led to different values of  $T_c$  and  $\xi_{GL}$  in the superconducting layers above and below this barrier. It is known that PMMA outgases significantly and that thinner lines are affected more [19]. This likely caused the observed line width dependence of the coupling strength and the complete oxidization of one of the superconducting layers for  $w \leq 120$  nm, where we found no evidence for two OPs. The critical Josephson current densities estimated from the inferred values of  $\gamma$  are consistent with this picture [25].

This fabrication result was unintentional but fortuitous. Due to the role of outgassing resist, it may be difficult to controllably tune parameters a priori in a similar process. Nevertheless, the data and analysis draw a clear picture of a two-OP superconductor with GL parameters that depend consistently on the ring line width. This dependence and the occurrence of two different  $T_c$ 's allowed the study of a wide range of parameters. The insight thus gained may be used for studies of intrinsic two-

component superconductors such as MgB<sub>2</sub> or Sr<sub>2</sub>RuO<sub>4</sub>. Fractional vortices in SrRu<sub>2</sub>O<sub>4</sub> would be of particular interest, as a  $p_x + ip_y$  OP would imply a zero energy core excitation with non-abelian braiding statistics [20]. Since their kinetic energy is logarithmically divergent in the sample size [2], they might only be accessible as metastable states in mesoscopic samples.

In conclusion, we have explored a range of effects related to the presence of two coupled order parameters in mesoscopic superconducting rings. The most interesting features of our results are an anomalous temperature dependence of the average superfluid density  $\lambda^{-2}$  and effective coherence length  $\xi_{GL}$ , and a qualitative modification of the behavior of phase slips related to metastable states with two different phase winding numbers.

This work was supported by NSF Grants No. DMR-0507931, DMR-0216470, ECS-0210877 and PHY-0425897 and by the Packard Foundation. Work was performed in part at the Stanford Nanofabrication Facility, which is supported by NSF Grant No. ECS-9731293, its lab members, and industrial affiliates. We would like to thank Per Delsing and Mac Beasley for useful discussions.

---

\* Electronic address: hendrikb@stanford.edu

- [1] C. Buzea and T. Yamashita, Superconductor Science & Technology **14**, R115 (2001).
- [2] E. Babaev, Phys. Rev. Lett. **89**, 067001 (2002).
- [3] Y. Tanaka, Phys. Rev. Lett. **88**, 017002 (2002).
- [4] A. Gurevich, Phys. Rev. B **67**, 184515 (2003).
- [5] C. Noce and L. Maritato, Phys. Rev. B **40**, 734 (1989).
- [6] P. G. Bjornsson, B. W. Gardner, J. R. Kirtley, and K. A. Moler, Rev. Sci. Inst. **72**, 4153 (2001).
- [7] P. G. D. Gennes, Rev. Mod. Phys. **36**, 225 (1964).
- [8] R. Meservey and B. B. Schwartz, *Equilibrium properties: comparison of experimental results with predictions of the BCS theory*. (New York, 1969), pp. 117 – 84.
- [9] R. B. Pettit and J. Silcox, Phys. Rev. B **13**, 2865 (1976).
- [10] R. W. Cohen and B. Abeles, Phys. Rev. **168**, 444 (1968).
- [11] J. Siegel, J. Witt, N. Venturi, and S. Field, Rev. Sci. Inst. **66**, 2520 (1995).
- [12] Attocube Systems AG, URL [www.attocube.com](http://www.attocube.com).
- [13] M. E. Huber et al., (unpublished).
- [14] V. Chandrasekhar, R. A. Webb, M. J. Brady, M. B. Ketchen, W. J. Gallagher, and A. Kleinsasser, Phys. Rev. Lett. **67**, 3578 (1991).
- [15] D. Mailly, C. Chapelier, and A. Benoit, Phys. Rev. Lett. **70**, 2020 (1993).
- [16] X. Zhang and J. C. Price, Phys. Rev. B **55**, 3128 (1997).
- [17] J. S. Langer and V. Ambegaokar, Phys. Rev. **164**, 498 (1967).
- [18] D. Y. Vodolazov, F. M. Peeters, S. V. Dubonos, and A. K. Geim, Phys. Rev. B **67**, 54506 (2003).
- [19] P. Dubos, P. Charlat, T. Crozes, P. Paniez, and B. Panetier, J. Vac. Sci. Technol. B **18**, 122 (2000).
- [20] M. Stone and S. Chung, cond-mat/0505513 (2005).
- [21] F. von Oppen and E. K. Riedel, Phys. Rev. B **46**, 3203 (1992).

- [22] N. C. Koshnick, H. Bluhm, M. E. Huber, and K. A. Moler, (unpublished).
- [23] Fluctuation effects within a few mK of  $T_c$  [21], where it would be inadequate to set  $\xi_{GL} = 0$ , will be discussed in Ref. [22].
- [24] For rings with  $R = 1 \mu\text{m}$ ,  $\Phi_a$  was too small to observe those features.
- [25] See auxiliary document at <http://www.stanford.edu/group/moler/publications.html> for a discussion of the fit procedures and parameters.